NTUA-92/00

QED in a Strong External Magnetic Field: Beyond the Constant Mass Approximation

J.Alexandre, K. Farakos, G. Koutsoumbas
Department of Physics, National Technical University of Athens,
Zografou Campus, 157 80 Athens, GREECE

arXiv:hep-ph/0004165v2 12 May 2000

Abstract

We solve the Schwinger-Dyson equations for QED in 2+1 or 3+1 dimensions in the presence of a strong homogeneous external magnetic field. The magnetic field is assumed strong enough, so that the lowest Landau level approximation holds, but the usual assumption of a momentum-independent self-energy is not made. In 2+1 dimensions, the scaling with logarithm changes to a square root dependence on the magnetic field, but the most spectacular result takes place in 3+1 dimensions, where the constant mass approximation turns out to be unreliable and the (momentum-dependent) dynamical mass is larger by several orders of magnitude compared to what has been found till now using the constant mass approximation.

1 Introduction

Magnetic catalysis of chiral symmetry breaking is well known by now as a concrete example of dynamical symmetry breaking, both in 2+1 and 3+1 dimensions. It is, of course, interesting from the field-theoretical point of view to have an example of dynamical symmetry breaking where explicit calculations may be performed. The non-perturbative tool used has been a consistent truncation of the SD equations based on the domination of the dynamics by the lowest Landau level (LLL) in the regime of strong magnetic fields. The results have shown that the presence of a homogeneous external magnetic field is enough to trigger dynamical mass generation even at very weak attractive coupling between the fermions.

The long history of the subject involves among others the very interesting issue of its role in models of the QCD vacuum [1] and a possible involvement in a new phase of QED with spontaneous chiral symmetry breaking, which has been claimed to offer an explanation of the e^+e^- pairs observed in the heavy ion experiments in GSI [2].

The Standard Electroweak Model in the presence of a constant magnetic field has been examined by Ambjorn and Olesen [3]. Their result is very briefly that, for strong enough magnetic field strength, they obtained a W and Z condensate solution and a lattice of vortex lines is formed, while at even stronger magnetic fields a phase transition to the symmetric phase takes place; the critical temperature needed for the symmetry restoration is substantially smaller than the one without magnetic field. Thus, it is seen that the magnetic field may induce a transition from the broken to the symmetric phase of the Electroweak Standard Model. These ideas of symmetry restoration in the presence of a magnetic field are discussed also earlier (see [4]).

The ground state of the electroweak theory has also been studied in the presence of a hypermagnetic field to the end of stregthening the electroweak phase transition so that it might give rise to baryogenesis within the Standard Model [5]. Moreover, the numerical work done and the contribution of ring diagrams in the effective potential show that the hypermagnetic field strengthening of the phase transition is not enough to satisfy all the standard model baryogenesis conditions.

Models for the formation of the strong magnetic fields that have been observed on the scale of galaxies are strongly based on the existence of extremely intense primordial magnetic fields [6]. These astrophysical and cosmological considerations are another field where magnetic field induced chiral symmetry breaking is relevant.

The model of a QED field theory with fermions has been suggested to describe the long-wavelength limit of the high-T_c superconducting cuprates [7]. Aspects of the behaviour of these materials, such as the scaling of their thermal conductivity, may find their explanation in the framework of the model under the influence of an external magnetic field [8].

The theory of dimensional reduction and magnetic catalysis has been developed by several groups [9, 10, 11, 12]. They have treated the problem of a constant external magnetic field acting on either Nambu Jona Lasinio model or QED in 2+1 or 3+1 dimensions. It was found that the magnetic field is actually a strong catalyst and even the weakest possible attraction between the fermions is enough for dynamical mass generation. In addition, in 2+1 dimensions, mass is generated dynamically for any number of flavours and not only for $N \leq 4$, as is the case without magnetic field [13] and the critical temperature for symmetry restoration is much smaller than $\sqrt{eB}$.

There have also been found solutions [14] of the Schwinger-Dyson equations in the limit

of weak magnetic field for (2+1)-dimensional QED with both quenched and dynamical fermions [14]. Also, if there is a coupling of the fermions to scalar fields in the presence of a magnetic field, a strong fermion condensate appears analogue to $\sqrt{eB}$ [15].

All of the above approaches have used the constant mass approximation, that is the self energy was supposed to be independent from the momentum. In this paper we try to make a step towards discarding this rather crude assumption and see the consequences in both the 2+1 and the 3+1 dimensional theories. To be able to proceed, we restrict ourselves to the strong field regime.

2 Fermions in a constant magnetic field

To fix our notations we shortly review here the characteristics of fermions in a constant external magnetic field, both in 2+1 and 3+1 dimensions.

The model we are going to consider is described by the Lagrangian density:

$$\mathcal{L} = -\frac{1}{4} f_{\mu\nu} f^{\mu\nu} + i\overline{\Psi} D_\mu \gamma^\mu \Psi - m\overline{\Psi}\Psi, \tag{1}$$

where $D_\mu = \partial_\mu + iga_\mu + ieA^{ext}_\mu$, a_μ is an abelian quantum gauge field, $f_{\mu\nu}$ is the corresponding field strength, and A^{ext}_μ describes an external electromagnetic field; in this work it will be a homogeneous magnetic field, constant in time. Notice that the fermions feel both the quantum and the external gauge fields, however we have allowed for different coupling constants, g and e. In three dimensions it makes sense to keep different couplings [7], while in 3+1 dimensions g is set equal to e. We recall the usual definition $g^2 \equiv 4\pi\alpha$.

We will choose the "symmetric" gauge

$$A^{ext}_1(x) = -\frac{B}{2} x_2, \quad A^{ext}_2(x) = +\frac{B}{2} x_1, \tag{2}$$

with the remaining components of the potential vanishing both in 2+1 and 3+1 dimensions. We notice for further reference that this potential has the property:

$$x^\mu A^{ext}_\mu(y) + y^\mu A^{ext}_\mu(x) = 0 \tag{3}$$

We know from the work of Schwinger [16] that the fermion propagator is given by:

$$S(x,y) = e^{iex^\mu A^{ext}_\mu(y)} \tilde{S}(x-y), \tag{4}$$

where the translational invariant propagator $\tilde{S}$ has the following Fourier transform:

$$\begin{aligned} \tilde{S}(p) &= \int_0^\infty ds \exp is \left(p_\parallel^2 - p_\perp^2 \frac{\tan(|eB|s)}{|eB|s} - m^2 \right) \\ &\times \left[(p^\parallel \gamma^\parallel + m)(1 + \gamma^1\gamma^2 \tan(|eB|s)) - p_\perp \gamma_\perp (1 + \tan^2(|eB|s)) \right] \end{aligned} \tag{5}$$

where $p^\perp \equiv (p^1, p^2)$, $p^\parallel \equiv p^0$ in 2+1 dimensions and $p^\parallel \equiv (p^0, p^3)$ in 3+1 dimensional space time. Similar notations hold for the γ-matrices.

There exists an additional representation for the fermion propagator, namely the Landau level expansion [17]. This expansion is particularly useful in the strong field regime, $|eB| >> m^2$,

since one may keep only the first term and get the so-called lowest Landau level approximation (LLL) [9, 18]:

$$\tilde{S}_{LLL}(p) = ie^{-p_\perp^2/|eB|}\frac{p^\parallel\gamma^\parallel + m}{p_\parallel^2 - m^2}\left(1 - i\gamma^1\gamma^2 sg(eB)\right) \tag{6}$$

It is this strong field regime that we will consider in this paper.

3 Schwinger-Dyson equation with an external magnetic field

The Schwinger-Dyson equation for the fermion propagator in d dimensions is given by the expression:

$$G(x,y) = S(x,y) - 4\pi\alpha\int d^dz_1 d^dz_2 d^dz_3 d^dz_4 S(x,z_1)\gamma^\mu G(z_1,z_2)\Gamma^\nu(z_2,z_3,z_4)G(z_4,y)\Delta_{\mu\nu}(z_3,z_1), \tag{7}$$

where G and $\Delta_{\mu\nu}$ are the full fermion and photon propagators and Γ^ν the full vertex. We show now perturbatively that G factors in the same way as the bare propagator S in equation (4), in other words it can be written in the form:

$$G(x,y) = e^{iex^\mu A_\mu^{ext}(y)}\tilde{G}(x-y). \tag{8}$$

Making a loop expansion in (7) and keeping only the tree level and the one loop terms we can write:

$$G(x,y) = S(x,y) - 4\pi\alpha\int d^dz_1 d^dz_2 S(x,z_1)\gamma^\mu S(z_1,z_2)\gamma^\nu S(z_2,y)D_{\mu\nu}(z_2,z_1) + ... \tag{9}$$

Note that we have used the bare vertex $\Gamma^\nu(z_2,z_3,z_4) = \gamma^\nu\delta(z_2-z_3)\delta(z_3-z_4)$, and that to this order in the loop expansion only the free photon $D_{\mu\nu}$ and fermion S propagators appear.

Let us now isolate the one-loop term in the expansion (9). This term reads:

$$\begin{aligned} G^{(1)}(x,y) &= -4\pi\alpha\int d^dz_1 d^dz_2 S(x,z_1)\gamma^\mu S(z_1,z_2)\gamma^\nu S(z_2,y)D_{\mu\nu}(z_2,z_1) \\ &= -4\pi\alpha\int d^dz_1 d^dz_2 \tilde{S}(x-z_1)\gamma^\mu\tilde{S}(z_1-z_2)\gamma^\nu\tilde{S}(z_2-y)D_{\mu\nu}(z_2-z_1) \\ &\quad\times\exp ie\left(x^\mu A_\mu^{ext}(z_1) + z_1^\mu A_\mu^{ext}(z_2) + z_2^\mu A_\mu^{ext}(y)\right) \end{aligned} \tag{10}$$

Using the change of variables $z_1 = y-u$, $z_2 = x+v$ and writing $r \equiv x-y$, we obtain:

$$\begin{aligned} G^{(1)}(x,y) &= -4\pi\alpha\int d^du d^dv \tilde{S}(r+u)\gamma^\mu\tilde{S}(-r-u-v)\gamma^\nu\tilde{S}(r+v)D_{\mu\nu}(r+u+v) \\ &\quad\times\exp ie\left(x^\mu A_\mu^{ext}(y-u) + (y-u)^\mu A_\mu^{ext}(x+v) + (x+v)^\mu A_\mu^{ext}(y)\right) \end{aligned} \tag{11}$$

Taking advantage of the property (3) of the potential A_μ^{ext}, we finally obtain:

$$G^{(1)}(x,y) = e^{iex^\mu A_\mu^{ext}(y)} \tilde{G}^{(1)}(r), \tag{12}$$

where

$$\tilde{G}^{(1)}(r) = -4\pi\alpha \int d^d u d^d v e^{iev^\mu A_\mu^{ext}(u)} \tilde{S}(r+u)\gamma^\mu \tilde{S}(-r-u-v)\gamma^\nu \tilde{S}(r+v) D_{\mu\nu}(r+u+v) \tag{13}$$

which is exactly equation (8). To be precise, the full propagator equals a phase times a translational invariant quantity. Proceeding the same way we can see that all the higher loop corrections behave as the one loop, showing perturbatively that G factorizes in the same way as S.

We can also see that the fermion self energy $\Sigma = G^{-1} - S^{-1}$ has also the same structure as S, since the Schwinger-Dyson equations can be written as:

$$\Sigma(x,y) = 4\pi\alpha\gamma^\mu \int d^d z_1 d^d z_2 G(x,z_1)\Gamma^\nu(y,z_1,z_2)\Delta_{\mu\nu}(z_2,x), \tag{14}$$

such that the one-loop self energy is:

$$\begin{aligned} \Sigma^{(1)}(x,y) &= 4\pi\alpha\gamma^\mu G(x,y)\gamma^\nu D_{\mu\nu}(y,x) \\ &= e^{iex^\mu A_\mu^{ext}(y)} \hat{\Sigma}(x-y) \end{aligned} \tag{15}$$

where $\hat{\Sigma}(r) = 4\pi\alpha\gamma^\mu \hat{G}(r)\gamma^\nu D_{\mu\nu}(r)$. The higher order corrections to Σ will have the same phase.

Since we will deal with the LLL approximation only, we cannot define the inverse of the fermion propagator (6) because of the projection operator $(1 - i\gamma^1\gamma^2)/2$; thus we cannot define the LLL approximation for $\Sigma(x,y)$. For this reason we will prefer to use the Schwinger-Dyson equation (7) and not (14). We will also take the bare vertex, so that our starting equation is:

$$G(x,y) = S(x,y) - 4\pi\alpha \int d^d z_1 d^d z_2 S(x,z_1)\gamma^\mu G(z_1,z_2)\gamma^\nu G(z_2,y)\Delta_{\mu\nu}(z_2,z_1) \tag{16}$$

We rewrite equation (16) in terms of the translational invariant fermion propagators $\tilde{S}(r)$ and $\tilde{G}(r)$

$$\tilde{G}(r) = \tilde{S}(r) - 4\pi\alpha \int d^d z_1 d^d z_2 \tilde{S}(r-z_1)\gamma^\mu \tilde{G}(z_1-z_2)\gamma^\nu \tilde{G}(z_2)\Delta_{\mu\nu}(z_2-z_1) e^{ie(r-z_2)^\mu A_\mu^{ext}(z_1)} \tag{17}$$

where $r = x - y$. Making a Fourier transform and performing the integration over z_1 we obtain:

$$\tilde{G}(k) = \tilde{S}(k) - 4\pi\alpha \tilde{I}(k), \tag{18}$$

where

$$\tilde{I}(k) = \int d^d z \int \frac{d^d p}{(2\pi)^d} \frac{d^d q}{(2\pi)^d} \tilde{S}(p-q+eA^{ext}(z))\gamma^\mu \tilde{G}(p)\gamma^\nu \tilde{G}(k-eA^{ext}(z))\Delta_{\mu\nu}(q) e^{iz(q-p+k)}. \tag{19}$$

We will look for a solution of (18) where the translational part of the full propagator reads in the spirit of the LLL approximation (equation (6)):

$$\tilde{G}_{LLL}(p) = ie^{-p_\perp^2/|eB|}\frac{Z_p p^\parallel \gamma^\parallel + M_p}{Z_p^2 p_\parallel^2 - M_p^2}\left(1 - i\gamma^1\gamma^2 sg(eB)\right), \tag{20}$$

where Z_p is the wave function renormalization and M_p the dynamically generated mass.

4 Magnetic catalysis in 2+1 dimensions

4.1 Integral equations

We will look for a solution of (18) with the expressions (6) with $m = 0$ and (20) substituted for the free and the full fermion propagator respectively. We are using four-component representation for the fermions and the γ matrices. To obtain the equations that Z_k and M_k must satisfy, we multiply $\tilde{I}(k)$ respectively by $(Z_k k^0\gamma^0 - M_k)$ and $\gamma^0(Z_k k^0\gamma^0 - M_k)$. We do a Wick rotation and then perform the integration over $z_0 = iz_3$, which leads to a factor $2\pi\delta(q_3 - p_3 + k_3)$. We obtain then the equations:

$$\begin{aligned}
\mathrm{tr}\left\{\left(Z_k ik_3\gamma^0 - M_k\right) I(k)\right\} &= -\frac{16i}{k_3}\int d^2z_\perp \int \frac{d^3p_E}{(2\pi)^3}\frac{d^2q_\perp}{(2\pi)^2}e^{\phi}\frac{Z_p p_3}{Z_p p_3^2 + M_p^2}\mathcal{D}(p_3 - k_3, q_\perp) \\
\mathrm{tr}\left\{\gamma^0\left(Z_k ik_3\gamma^0 - M_k\right) I(k)\right\} &= -\frac{16}{k_3}\int d^2z_\perp \int \frac{d^3p_E}{(2\pi)^3}\frac{d^2q_\perp}{(2\pi)^2}e^{\phi}\frac{M_p}{Z_p p_3^2 + M_p^2}\mathcal{D}(p_3 - k_3, q_\perp),
\end{aligned}$$

where $\phi \equiv iz_\perp(q_\perp - p_\perp + k_\perp) - \frac{1}{|eB|}\left[(p_\perp - q_\perp + eA^{ext}(z))^2 + p_\perp^2 + (k_\perp - eA^{ext}(z))^2\right]$ and $\mathcal{D}(q_3, q_\perp) = -iD_{00}(q_E)$. We note that only the component D_{00} of the photon propagator plays a role in the Schwinger-Dyson equations, due to the projection operator $(1 - i\gamma^1\gamma^2)/2$ which appears in the fermion propagators when the LLL approximation is used.
The integrations over $p_\perp$ and $z_\perp$ are straightforward. We also have the auxiliary relations:

$$\begin{aligned}
\mathrm{tr}\left\{\left(Z_k ik_3\gamma^0 - M_k\right)\left(\tilde{G}(k) - \tilde{S}(k)\right)\right\} &= 4ie^{-k_\perp^2/|eB|}(1 - Z_k) \\
\mathrm{tr}\left\{\gamma^0\left(Z_k ik_3\gamma^0 - M_k\right)\left(\tilde{G}(k) - \tilde{S}(k)\right)\right\} &= 4e^{-k_\perp^2/|eB|}\frac{M_k}{k_3},
\end{aligned}$$

such that (18) yields the final integral equations:

$$\kappa(1 - Z_\kappa) = \frac{\tilde{\alpha}}{\pi}\int_{-\infty}^{\infty} dv \int_0^\infty du e^{-u^2/2}\frac{uvZ_v}{Z_v^2 v^2 + \mu_v^2}\mathcal{D}(v - \kappa, u) \tag{21}$$

$$\mu_\kappa = \frac{\tilde{\alpha}}{\pi}\int_{-\infty}^{\infty} dv \int_0^\infty du e^{-u^2/2}\frac{u\mu_v}{Z_v^2 v^2 + \mu_v^2}\mathcal{D}(v - \kappa, u) \tag{22}$$

We have introduced the dimensionless variables $\tilde{\alpha} \equiv \alpha/\sqrt{|eB|}$, $u \equiv \sqrt{q_\perp^2/|eB|}$, $v \equiv p_3/\sqrt{|eB|}$, $\kappa \equiv k_3/\sqrt{|eB|}$ and $\mu_\kappa \equiv M_k/\sqrt{|eB|}$. The reader can check that the integral equations (21, 22) are consistent with the ones in [12]. We note that μ_κ and Z_κ depend only on the dimensionless ratio $\tilde{\alpha}$.

The free photon propagator $\Delta_{\mu\nu}$ will be used, since we show in the appendix that it receives no corrections in this case. In particular, it is shown that the one-loop polarization tensor is suppressed by $\alpha|eB|^{-1/2}$, such that in the LLL approximation we will use in (21, 22) the Euclidean photon propagator

$$\mathcal{D}(v-\kappa,u)=\frac{1}{u^2+(v-\kappa)^2}\left(1-\frac{(v-\kappa)^2}{u^2+(v-\kappa)^2}\right)+\lambda\frac{(v-\kappa)^2}{\left(u^2+(v-\kappa)^2\right)^2} \tag{23}$$

where λ is the gauge fixing parameter.

4.2 Constant mass approximation

Before proceeding with a detailed analysis of (21, 22), we start with a first approximation, which consists in setting $Z_v=1$ and a constant dynamical mass μ_c in the integral equations, so that in the Feynman gauge $\lambda=1$ equation (22) reads:

$$\mu_\kappa^{const}=\frac{\tilde{\alpha}}{\pi}\int_{-\infty}^{\infty}dv\int_0^{\infty}due^{-u^2/2}\frac{u\mu_c}{v^2+\mu_c^2}\frac{1}{u^2+(v-\kappa)^2} \tag{24}$$

The integration over v is done by the residue theorem and leads to:

$$\mu_\kappa^{const}=\tilde{\alpha}\int_0^{\infty}due^{-u^2/2}\frac{u+\mu_c}{\kappa^2+(u+\mu_c)^2} \tag{25}$$

Thus the constant dynamical mass is obtained by solving the equation $\mu_{\kappa=0}^{const}=\mu_c$ which reads:

$$\mu_c=\tilde{\alpha}\int_0^{\infty}due^{-u^2/2}\frac{1}{u+\mu_c} \tag{26}$$

The study of (26) has also been done in [8].
Putting $Z_v=1$ as a first approximation and taking a constant mass in equation (22) leads to the following second approximation to Z_κ :

$$Z_\kappa^{const}=1-\tilde{\alpha}\int_0^{\infty}due^{-u^2/2}\frac{1}{\kappa^2+(u+\mu_c)^2}, \tag{27}$$

such that its value for zero momentum is given by:

$$Z_c=1-\tilde{\alpha}\int_0^{\infty}due^{-u^2/2}\frac{1}{(u+\mu_c)^2}. \tag{28}$$

We plot the dimensionless dynamical mass gap $\tilde{\alpha}^{-1}\mu_c/Z_c$ versus $\sqrt{|eB|}/\alpha$ in figure 3 and compare with the mass gap obtained with $\mu_{\kappa=0}$ and $Z_{\kappa=0}$ solutions of (21,22) that we find in the next section. We can see that the constant mass approximation leads to an over-evaluation of the dynamical mass gap and that it gets worse as the magnetic field increases.

4.3 Momentum dependent solutions

We now concentrate on the momentum dependence of the dynamical mass and the wave function renormalization to obtain a more precise analysis of the solution of (21,22).
Let us first study the wave function renormalization Z_κ. We will actually consider the one-loop approximation, consistently with our treatment of the Schwinger-Dyson equation (7), where we considered the bare vertex. Since there is no pertubative solution of the integral equations for the dynamical mass μ_κ, our numerical solution of the system of integral equations will correspond to some resummation of diagrams. The solution will be found through an iterative procedure: a trial function will be put in equations (21, 22) to yield a first estimate of Z_κ and μ_κ. We will then take this output and substitute it back in the right hand sides of the integral equations to obtain better approximations. As we will see, this iterative procedure does finally converge to a solution.
The trial function will be given by the solution of a differential equation verified by μ_κ that will be derived now. This differential equation is derived also in [9] for the (3+1)-dimensional model in what they called linearized approximation.

Let us now proceed with equation (22). We start by splitting the integration over v in (22) in two parts:

$$\begin{aligned}\mu_\kappa &\simeq \frac{\tilde{\alpha}}{\pi}\int_{|v|<\kappa} dv \int_0^\infty du e^{-u^2/2}\frac{u\mu_v}{Z_v^2 v^2+\mu_v^2}\mathcal{D}(\kappa,u)\\ &+ \frac{\tilde{\alpha}}{\pi}\int_{|v|>\kappa} dv \int_0^\infty du e^{-u^2/2}\frac{u\mu_v}{Z_v^2 v^2+\mu_v^2}\mathcal{D}(v,u) \qquad (29)\end{aligned}$$

Notice the approximations used: $\mathcal{D}(v-\kappa,u)\approx\mathcal{D}(\kappa,u)$ for $|v|<\kappa$ and $\mathcal{D}(v-\kappa,u)\approx\mathcal{D}(v,u)$ for $|v|>\kappa$. Then the derivative with respect to κ leads to the following equality:

$$\mu'_\kappa \equiv \frac{d\mu_\kappa}{d\kappa} = \frac{2\tilde{\alpha}}{\pi} f_\kappa \int_0^\kappa dv \frac{\mu_v}{Z_v^2 v^2+\mu_v^2} \qquad (30)$$

where we defined:

$$f_\kappa \equiv \frac{d}{d\kappa}\left\{\int_0^\infty du e^{-u^2/2} u\mathcal{D}(\kappa,u)\right\} \qquad (31)$$

A new derivative with respect to κ finally gives:

$$f_\kappa\mu''_\kappa - f'_\kappa\mu'_\kappa - \frac{2\tilde{\alpha}}{\pi}f_\kappa^2\frac{\mu_\kappa}{Z_\kappa^2\kappa^2+\mu_\kappa^2} = 0 \qquad (32)$$

From now on we take $Z_\kappa = 1$ in (32). We should stress that this differential equation is only approximate, and the approximation (29) is not controled by any small parameter. Since we have no full control on the assumptions made, we consider the solution of (32) only as a trial function which could help us with the solution of the integral equations. It turns out that the iterative procedure described above converges quickly yielding a solution for Z_κ and μ_κ reproducing itself after a small number of steps. This may be seen in figure 1 for μ_κ. We find that the convergence of Z_κ is even quicker. It turns out that the solution found as the limit of the iterative procedure does not depend on the trial function μ_κ that one starts with; however,

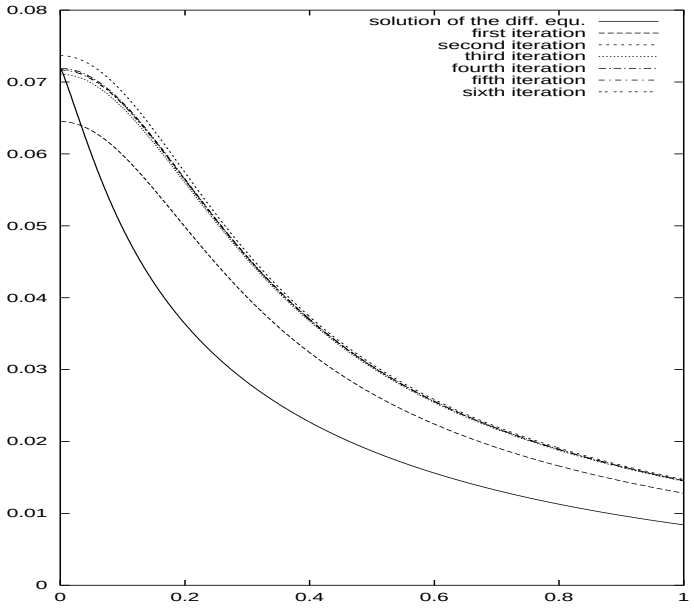

Figure 1: μ_κ versus κ for $\tilde{\alpha} = .03$ (d=2+1)

taking the solution of the differential equation gives a much better convergence, that is the speed of convergence is increased. As can be seen on figure 1, μ_κ is almost flat for $\kappa < \mu_{\kappa=0}$, as was also emphasized in [9] for 3+1 dimensions.

To solve (32), we needed the initial conditions that the function μ_κ has to satisfy. Suppose that $\mu_{\kappa=0} = \mu_0$. In the Feynman gauge, the function f_κ has the following behaviour around $\kappa = 0$

$$f_\kappa \sim -\frac{1}{\kappa} \quad \text{as } \kappa \to 0 \tag{33}$$

Thus if we wish μ''_κ to be finite in $\kappa = 0$, (32) implies that:

$$\mu'_{\kappa=0} = -\frac{2\tilde{\alpha}}{\pi\mu_0}. \tag{34}$$

Next we have to determine μ_0. We invoke the fact that $\mu_\kappa \to 0$ as $\kappa \to \infty$ and thus choose μ_0 such that $\lim_{\kappa\to\infty} \mu_\kappa = 0$. As a side remark we note here that the trial function we obtain is not an even function of κ; this is a consequence of the approximations made to get the differential equation (32). The even function μ_κ is found after plugging the trial function into the integral equations (21, 22). Equation (32) has been solved numerically through the use of a fourth order Runge-Kutta method. The estimate of the function f_κ as well as its derivative has been done using a Gauss-Hermite quadrature of order 40.

In figure 2 we plot the dimensionless mass gap μ_κ/Z_κ as a function of the dimensionless momentum κ. One of the curves comes from the solution of the integral equations (using the iterative procedure), while for the sake of comparison we also plot the solution of the differential equation (32). We note that in the differential equation we have set $Z_\kappa = 1$; on the contrary, Z_κ changes during the iterative procedure for the solution of the integral equations. We observe that the quantity μ_κ/Z_κ derived from the differential equation is very close to its final value that is found after substituting it the integral equations. This explains why the iterative procedure

converges fast if we use μ_κ as input. It is obvious from the figure that the mass gap decreases rather rapidly with increasing momentum and takes its maximum value for $\kappa = 0$. Thus it is to be expected that we will have big differences from the constant mass approximation, which assumes the same value for $0 \leq \kappa < \infty$. The small momenta will be given the major role, in accordance with the fact that mass generation is an infrared phenomenon.

In figure 3 we try to get contact with [8] and plot the dimensionless dynamical mass $\mu/\tilde{\alpha} = M/\alpha$ versus $\sqrt{|eB|}/\alpha$ for two cases: the constant mass approximation obtained from (26) and the momentum dependent version, coming from the solutions of the integral equations (21,22).

In the constant mass case, we find a logarithmic fit, which reads:

$$\tilde{\alpha}^{-1}\mu^{fit}_{const} = m_0 \ln \frac{\sqrt{|eB|}}{\alpha} \qquad \text{with} \qquad m_0 \simeq .765 \pm .001 \tag{35}$$

or

$$\mu^{fit}_{const} = m_0 \frac{\alpha}{\sqrt{|eB|}} \ln \frac{\sqrt{|eB|}}{\alpha} \tag{36}$$

in agreement with the result of [8].

For the momentum dependent solution, we choose to plot the value of this dynamical mass at $\kappa = 0.$ versus $|eB|$. The fit now is dramatically modified and reads:

$$\tilde{\alpha}^{-1}\mu^{fit}_{\kappa=0} = m_1 + m_2 \frac{\sqrt{|eB|}}{\alpha} \quad \text{with} \quad m_1 = 2.65 \pm .01 \ \text{ and } \ m_2 = (2.1 \pm 0.1) \times 10^{-4} \tag{37}$$

Of course, changing a logarithm to a square root is a fundamental difference from the previous case. We also observe the quantitative change in the value of the mass in comparison to the constant mass approximation: for the magnetic fields which are plotted in figure 3, the mass is smaller by a factor of two to three. We should stress that the above results have been produced using the lowest Landau level approximation, which holds provided the magnetic field is strong. This means that our results, shown in figure 3, should not be trusted in the region near the origin of the horizontal axis. In this respect we observe in the figure that the data for the momentum dependent mass are well represented by the above fit in the region of large magnetic fields down to the value $\sqrt{|eB|}/\alpha \simeq 100$. We may interprete this change of behaviour of the data for small magnetic fields as been due to the LLL approximation, which is poor in this region; this may yield an estimate of the limit of its validity. We note here that with zero magnetic field, the dynamical mass obtained by the Schwinger-Dyson equation in the constant mass approximation is bigger than the mass obtained solving the equations using a momentum dependent self energy for the fermion [13].

4.4 Fermion condensate

The fermion condensate is given by

$$\left\langle 0|\overline{\psi}\psi|0\right\rangle = \lim_{y\to x} \mathrm{tr} G(x,y) = \mathrm{tr} \int \frac{d^3p}{(2\pi)^3} \tilde{G}(p), \tag{38}$$

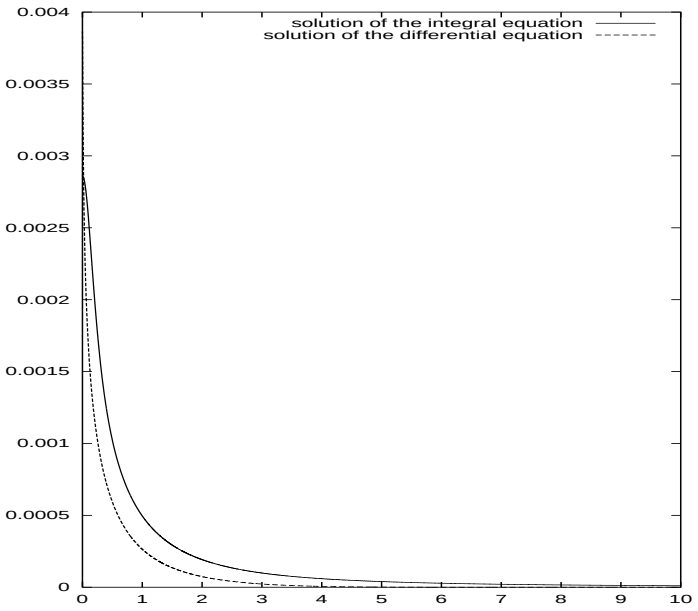

Figure 2: μ_κ/Z_κ versus κ for $\tilde{\alpha} = .001$ (d=2+1)

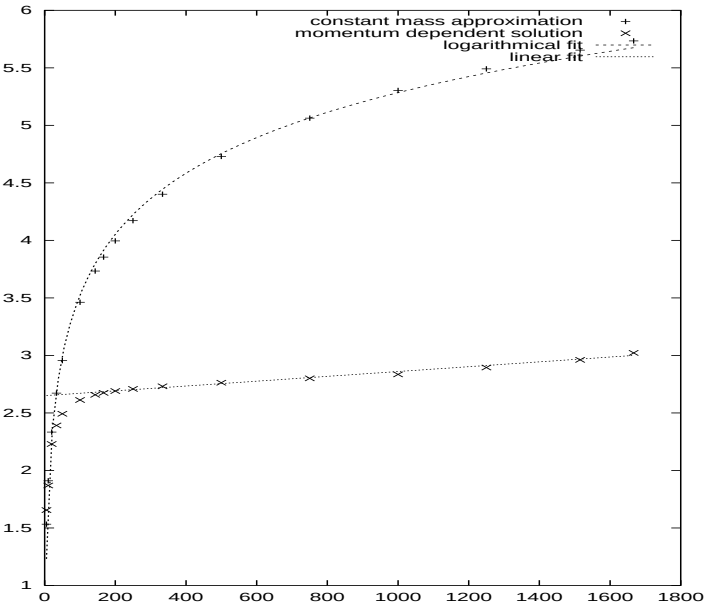

Figure 3: Dimensionless mass gap $\mu/\tilde{\alpha}$ versus $\sqrt{|eB|}/\alpha$ (d=2+1)

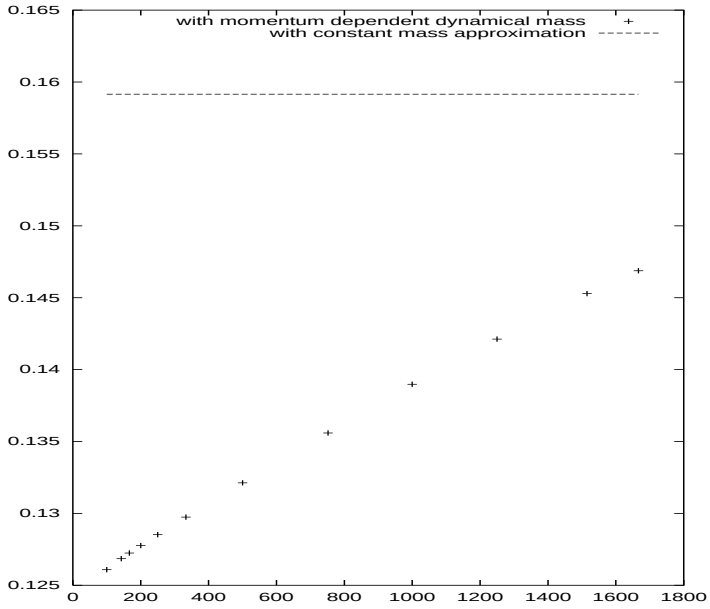

Figure 4: Dimensionless fermion condensate $< 0|\overline{\psi}\psi|0 > /|eB|$ versus $\sqrt{|eB|}/\alpha$ (d=2+1)

which, in the LLL approximation, leads to:

$$\begin{aligned} \left\langle 0|\overline{\psi}\psi|0\right\rangle &= -4i\int \frac{d^2p_\perp}{(2\pi)^2} e^{-p_\perp^2/|eB|} \int \frac{idp_3}{2\pi} \frac{M_p}{Z_p^2 p_3^2 + M_p^2} \\ &= \frac{|eB|}{2\pi^2}\int_{-\infty}^{\infty} dv \frac{\mu_v}{Z_v^2 v^2 + \mu_v^2}. \end{aligned} \tag{39}$$

In the constant mass approximation with $Z_v = 1$ the integral (39) yields the simple result:

$$\left\langle 0|\overline{\psi}\psi|0\right\rangle = \frac{|eB|}{2\pi}. \tag{40}$$

It is worth noting that in this approximation the condensate does not depend on the dynamical mass μ_v. The condensate in the constant mass approximation grows linearly with $|eB|$ with a slope equal to $1/(2\pi) \simeq 0.1592$. We compared (40) with the condensate given by equation (39) using the momentum dependent functions μ_v and Z_v found numerically in the previous subsection. We show in figure 4 the dimensionless condensate $\left\langle 0|\overline{\psi}\psi|0\right\rangle /|eB|$ versus $\sqrt{|eB|}/\alpha$, both for the momentum dependent and the constant mass solutions. We see that the condensate varies linearly over a wide range of $\sqrt{|eB|}/\alpha$. We remark that the fermion condensate does not vanish in the limit $|eB| \to 0$ in 2+1 dimensions [13], but we cannot explore this limit within the LLL approximation, which is only reliable for strong magnetic fields.

5 Magnetic catalysis in dimension d=3+1

5.1 Integral equations

The techniques used in the (3+1)-dimensional model are similar to the ones developed in the previous section, so we will only give the results.
Starting again from the Schwinger-Dyson equations (7), we obtain in the same way as before

$$\begin{aligned}\kappa^2(1-Z_\kappa) &= \frac{\alpha}{\pi^2}\int d^2v\int_0^\infty du e^{-u^2/2}\frac{uZ_v\vec{\kappa}.\vec{v}}{Z_v^2v^2+\mu_v^2}\mathcal{D}(\vec{v}-\vec{\kappa},u)\\ \mu_\kappa &= \frac{\alpha}{\pi^2}\int d^2v\int_0^\infty du e^{-u^2/2}\frac{u\mu_v}{Z_v^2v^2+\mu_v^2}\mathcal{D}(\vec{v}-\vec{\kappa},u)\end{aligned} \tag{41}$$

where now $\vec{\kappa}$ is the two dimensional vector representing two components of the dimensionless Euclidean momentum:

$$\vec{\kappa}=\frac{1}{\sqrt{|eB|}}(k_4,k_3)=\frac{1}{\sqrt{|eB|}}(-ik_0,k_3) \tag{42}$$

In 3+1 dimensions, the corrections to the photon propagator are not suppressed by inverse powers of the magnetic field, so we use the expression [9]:

$$D_{\mu\nu}(q)=-i\frac{g^{\parallel}_{\mu\nu}}{q^2+q_\parallel^2\Pi(q_\perp^2,q_\parallel^2)}-i\frac{g^{\perp}_{\mu\nu}}{q^2}+i\frac{q^\perp_\mu q^\perp_\nu+q^\perp_\mu q^\parallel_\nu+q^\parallel_\mu q^\perp_\nu}{q^4}, \tag{43}$$

where $\Pi(q_\perp^2,q_\parallel^2)$ is the polarization tensor and $g^\parallel_{\mu\nu}$ and $g^\perp_{\mu\nu}$ represent the restrictions of the metric tensor to the $(3,4)$ and $(1,2)$ directions respectively. Because of the projection operator $(1-i\gamma^1\gamma^2 sg(eB))/2$, appearing in the fermion propagator in the LLL approximation, only the part of $D_{\mu\nu}$ containing $g^\parallel_{\mu\nu}$ will contribute to the Schwinger-Dyson equations. Therefore we will only have to consider the expression

$$D^{LLL}_{\mu\nu}(q)=-i\frac{g^\parallel_{\mu\nu}}{q^2+q_\parallel^2\Pi(q_\perp^2,q_\parallel^2)}, \tag{44}$$

where we will use for the polarization tensor the form [11]:

$$q_\parallel^2\Pi(q_\parallel^2,q_\perp^2)\simeq-\frac{2\alpha|eB|}{\pi}e^{-q_\perp^2/(2|eB|)}, \tag{45}$$

α being the QED coupling renormalized at the scale $\sqrt{|eB|}$. Actually the approximation (45) is valid only for $q_\parallel^2>>M^2$ where M is the dynamical mass of the fermions, but the latter will be very small compared to the typical momenta we will consider, so the approximation is good. Therefore the photon propagator in dimension 3+1 will be:

$$D^{LLL}_{\mu\nu}(q)=-i\frac{g^\parallel_{\mu\nu}}{q^2-\frac{2\alpha}{\pi}|eB|e^{-q_\perp^2/(2|eB|)}}, \tag{46}$$

such that the quantity $\mathcal{D}(\vec{v}-\vec{\kappa},u)$ in (41) will be replaced by:

$$\mathcal{D}(\vec{v}-\vec{\kappa},u)=\frac{1}{u^2+(\vec{v}-\vec{\kappa})^2+\frac{2\alpha}{\pi}e^{-u^2/2}} \tag{47}$$

The integral equation for μ_κ is consistent with the results of [9] where the authors do not consider the contribution of the wave function renormalization. It is known that in the dynamical symmetry breaking in QED, without external field, Z_κ is equal to one, if we employ the Landau gauge [19, sect.8.4]. However, with an external magnetic field, the photon propagator (46) is such that we find $Z_\kappa \neq 1$ as can be seen in figure 6.

5.2 Constant mass approximation

We first have a look at the constant mass approximation of (41), to facilitate comparison with [9]; we do not consider in this subsection the corrections to the photon propagator. Denoting $\rho \equiv \vec{\kappa}^2$, we consider the integral equation for $\rho = 0$ and $Z_v = 1$ and set $\mu_\rho = \mu_v = \mu_c$. The integration over v then leads to the following gap equation:

$$1 = \frac{\alpha}{\pi} \int_0^\infty du e^{-u^2/2} \frac{u}{\mu_c^2 - u^2} \ln\left(\frac{\mu_c^2}{u^2}\right) \tag{48}$$

We plot in figure 5 the dynamical mass obtained from (48) as well as the analytical estimate of [9], which is:

$$\mu_c^{analyt} = C \exp\left[-\frac{\pi}{2}\left(\frac{\pi}{2\alpha}\right)^{1/2}\right] \tag{49}$$

and choose $C = 1$. We can see that this estimate agrees very well with our results. But we will see in the next paragraph that the momentum dependent dynamical mass gives completely different results from the constant mass approximation in 3+1 dimensions, which was not the case in 2+1 dimensions. From the numerical point of view, this comes from the fact that in 3+1 dimensions the dimensionless dynamical mass μ_c is not present in the left-hand side of the gap equation (48), contrary to what happened in (26), the corresponding equation in 2+1 dimensions. The result is that the order of magnitude of the integral should be $1/\alpha$ in 3+1 dimensions. This pushes the integral to very big values, that can be obtained by extremely small values for μ_c. On the other hand, such problems are not present for the momentum dependent solution; this leads to a serious discrepancy, by several orders of magnitude, between the momentum dependent solution of (41) and the constant mass approximation which therefore is not reliable in 3+1 dimensions. We note that this fact is independent of our taking into account Z_κ, since the latter is very close to 1 and thus cannot give a change of several orders of magnitude (see figure 6). We also note that such problems do not arise in 2+1 dimensions, since, by equation (26), the order of magnitude of the integral is $\mu_c/\tilde{\alpha}$ in this case, so the smallness of $\tilde{\alpha}$ is compensated by a small number, such as μ_c; thus moving to a momentum dependent solution in 2+1 dimensions brings in some quantitative differences but not the huge ones characterising the 3+1 dimensions. It seems that the constant mass approximation in 2+1 dimensions is relatively reliable.

5.3 Momentum dependent solutions

We are looking for solutions of (41) which are even functions of the momentum. Thus we consider μ and Z as functions of the variable $\rho \equiv \kappa^2 = k^2/|eB|$. The differential equation similar to (32) is then obtained in the same way and reads:

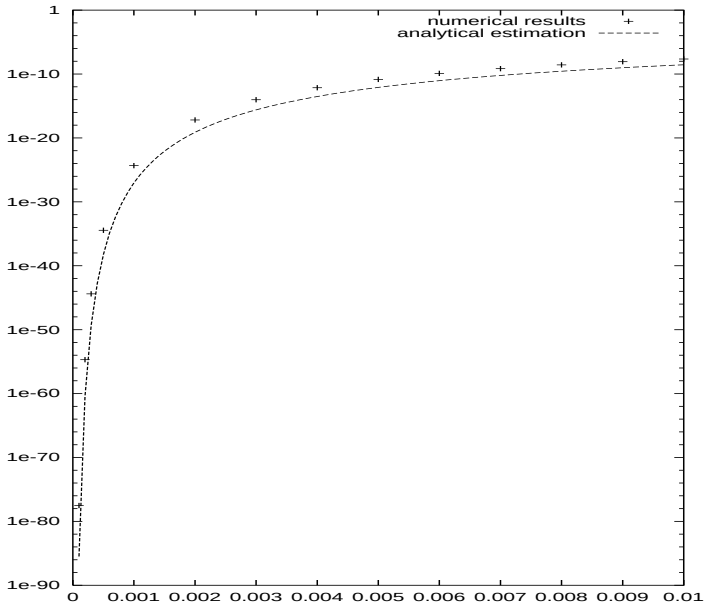

Figure 5: Dimensionless dynamical mass μ_c versus α in the constant mass approximation (d=3+1)

$$f_\rho \mu_\rho'' - f_\rho' \mu_\rho' - \frac{\alpha}{\pi} f_\rho^2 \frac{\mu_\rho}{Z_\rho^2 \rho + \mu_\rho^2} = 0 \tag{50}$$

where the function f_ρ is given by

$$f_\rho = \frac{d}{d\rho} \left\{ \int_0^\infty du e^{-u^2/2} u \mathcal{D}(\sqrt{\rho}, u) \right\}. \tag{51}$$

Equation (50) is consistent with the one given in [9] and we will set $Z_\rho = 1$ to solve it.
Coming back to the integral equations (41), we can perform the $\vec{v}$-angular integration if we look for functions μ_ρ and Z_ρ depending on ρ only. The result reads:

$$\begin{aligned} Z_\rho^{(1)} &= 1 + \frac{\alpha}{2\pi\rho} \int_0^\infty dv \int_0^\infty du e^{-u^2/2} \frac{u}{v + \mu_v^2} \left[1 - \frac{u^2 + \rho + v + 2\alpha/\pi \exp(-u^2/2)}{\sqrt{\left(u^2 + \rho + v + 2\alpha/\pi \exp(-u^2/2)\right)^2 - 4\rho v}} \right] \\ \mu_\rho &= \frac{\alpha}{\pi} \int_0^\infty dv \int_0^\infty du e^{-u^2/2} \frac{u \mu_v}{Z_v^2 v + \mu_v^2} \frac{1}{\sqrt{\left(u^2 + \rho + v + 2\alpha/\pi \exp(-u^2/2)\right)^2 - 4\rho v}}, \end{aligned} \tag{52}$$

where we have used the one-loop approximation $Z_\rho^{(1)}$ for the wave function renormalization Z_v.

We solve numerically (52) in the same way as we solved the equivalent set of equations in dimension 2+1. We first solve the differential equation (50) and use the solution as a trial function for the integral equations (52). Then the outcome is used as feedback in the integral equations (6) and the resulting iterative procedure is converging, somehow slower as compared to 2+1 dimensions. To find the initial conditions of μ_ρ satisfying (50), we note that:

$$f_\rho \sim -\frac{1}{2\rho} \quad \text{when } \rho \to 0, \tag{53}$$

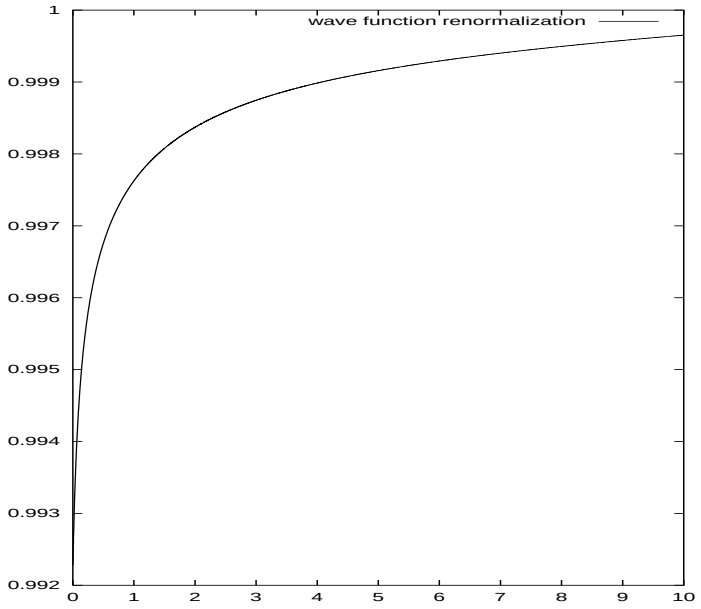

Figure 6: Wave function renormalization Z_ρ versus ρ for $\alpha = .01$ (d=3+1)

so that (50) implies that:

$$\mu'_{\rho=0} = -\frac{\alpha}{2\pi\mu_0} \quad \text{with} \quad \mu_0 \equiv \mu_{\rho=0}, \tag{54}$$

if we demand that μ_ρ is twice differentiable as $\rho \to 0$. We then find μ_0 by imposing the condition $\lim_{\rho\to\infty} \mu_\rho = 0$, as we did in 2+1 dimensions.
In figure 7 we depict the evolution of the dimensionless dynamical mass at zero momentum, $\mu_{\kappa=0}$, with the coupling α, as well as a fit which is given by:

$$\mu^{fit}_{\rho=0} = \mu_0\sqrt{\alpha} \qquad \text{with} \qquad \mu_0 = .0300 \pm 0.0001 \tag{55}$$

The dimensionless mass gap $(\mu_\rho/Z_\rho)_{\kappa=0}$ follows the same fit, since $Z_\rho \simeq 1$. We may compare figures 5 and 7 and see the huge difference (by some orders of magnitude) between the constant mass approximation and the momentum dependent solution in 3+1 dimensions. The first conclusion is of course the that one cannot really trust the constant mass approximation, as already stated above. However, such a change will make itself felt and, if this analysis is correct, the relevant chiral symmetry breaking triggered by external magnetic fields should have measurable physical consequences.

5.4 Fermion condensate

The fermion condensate in the LLL approximation is given by:

$$\left\langle 0|\overline{\psi}\psi|0\right\rangle = \frac{|eB|^{3/2}}{4\pi^2}\int_0^\infty d\rho \frac{\mu_\rho}{Z^2_\rho\rho + \mu^2_\rho} \tag{56}$$

Since we compute the condensate with the momentum dependent mass and wave function renormalization, we do not have to compensate any divergence: the condensate is convergent.

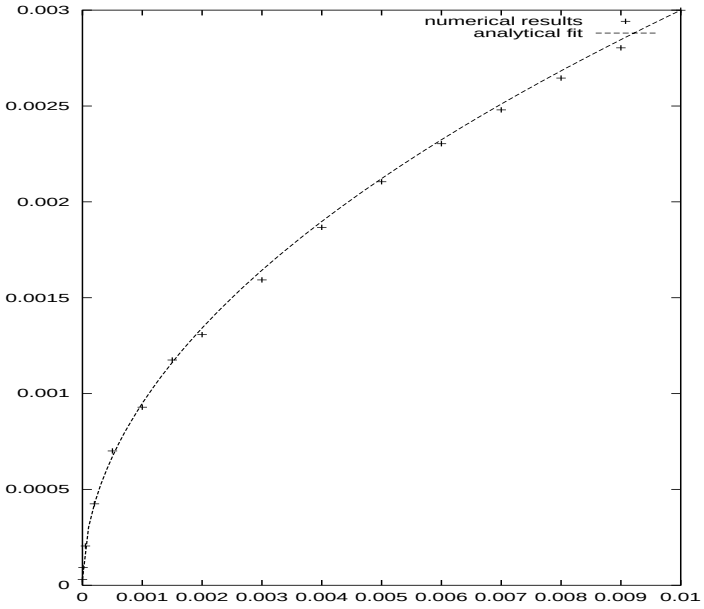

Figure 7: Dimensionless dynamical mass $\mu_{\rho=0}$ versus α (d=3+1)

In a perturbative expansion, the condensate has to be renormalized to any order but here we started from the Schwinger-Dyson equation which is non-perturbative and leads us to a convergent resummation of graphs for the condensate. We can note that the divergence in the computation of the fermion condensate for the constant mass approximation can be removed if we substract the condensate for $|eB| = 0$. We obtain then a convergent expression which vanishes as $m^2 \to 0$. To see this, let us go back to the Schwinger representation (5) of the fermion propagator and take away the gauge dynamics, putting $\alpha \to 0$. The computation of the condensate is straightforward [20] and leads to:

$$\left\langle 0|\overline{\psi}\psi|0\right\rangle - \left\langle 0|\overline{\psi}\psi|0\right\rangle_{|eB|=0} = \frac{m|eB|}{4\pi^2}\int_0^\infty \frac{ds}{s}e^{-s}\left[\coth\left(s\frac{|eB|}{m^2}\right) - \frac{m^2}{s|eB|}\right] \tag{57}$$

In our numerical study with zero bare mass, we also find a vanishing condensate for $\alpha \to 0$, at least for strong magnetic fields since we only considered the LLL approximation. Thus in this approximation we do not find any critical coupling for the condensate to be generated. We plot in figure 8 the dimensionless fermion condensate $c_f = B^{-3/2}\left\langle 0|\overline{\psi}\psi|0\right\rangle$ versus the coupling α, taking into account the relation $e^2 = 4\pi\alpha$.

We note that the analytical approximation of the fermion condensate given in [18] does not fit to our numerical results. The difference lies in their taking the constant mass approximation and a cut-off $|eB|$ in the momentum space. Instead we found the analytical fit:

$$c_f^{fit} = c_0\ \alpha^{1/4} \qquad \text{with} \qquad c_0 = .00590 \pm 0.00001 \tag{58}$$

for the dimensionless fermion condensate.

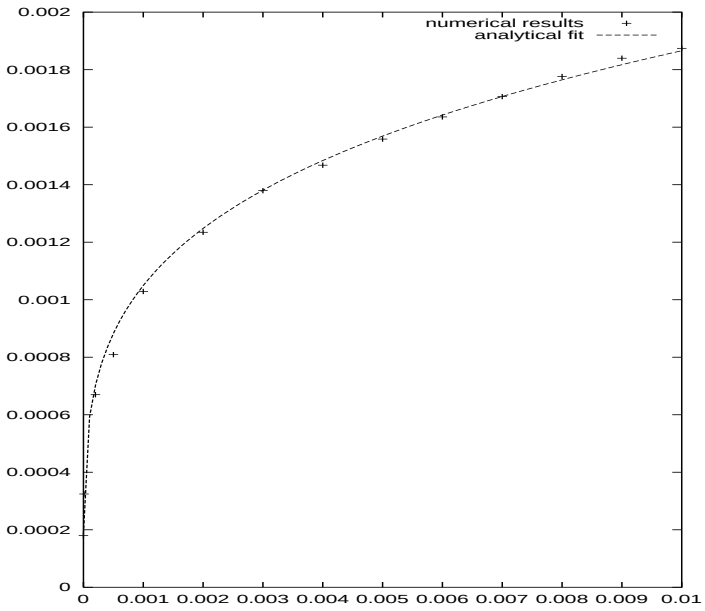

Figure 8: Dimensionless fermion condensate $B^{-3/2} < 0|\overline{\psi}\psi|0 >$ versus α (d=3+1)

6 Conclusions

Our results for the (2+1)-dimensional model are relevant for condensed matter Physics, in particular models for high-T_c superconductivity, while the (3+1)-dimensional case has to do with the Electroweak Phase Transition in the Early Universe.

- As we already stated in the beginning, there has been a suggestion [7, 8] that the high-T_c superconducting materials can be described by an effective theory, namely a relativistic gauge field theory in 2+1 dimensions. The complete model was $SU(2) \times U(1)$ symmetric with a doublet of massless fermions [22]. However, simpler versions, such as QED in 2+1 dimensions have been studied in the same context. The theory describes the quasi-particle excitations about the nodes of a d-wave superconducting gap. The Fermi velocity coincides with the effective velocity of light. In a recent experiment [23] it has been found that for strong magnetic fields (about O(1) to O(10) Tesla) there appear plateaus in the thermal conductivity of the material, signalling the opening of a new gap at the nodes, induced by the magnetic field. The critical temperature T_{crit} for the appearance of this superconducting gap scales with the magnetic field as $T_{crit} \approx \sqrt{|eB|}$. Assuming that the critical temperature (where the dynamical mass vanishes) is roughly proportional to the dynamical mass at zero temperature, we see that our equation (37), which says that the dynamical mass scales as $\sqrt{|eB|}$, agrees with this experimental result. Of course, a true finite temperature calculation must be done if a better founded assertion can be made.

- Concerning the dynamical mass generation and the fermionic condensate in 3+1 dimensions, we mention that around the Electroweak era magnetic fields of the order of $10^{23} - 10^{24}$ are naturally obtained [6]. These correspond to a dynamical mass of the order of 1GeV, if we set $\frac{e^2}{4\pi} \simeq \frac{1}{137}$, independently from the vacuum expectation value of the

scalar field. This is already a big value for the mass with eventually observable contribution in the effective potential at high temperature. However, if we want to give an explanation for the galactic magnetic fields (of the order of 10^{-6} Gauss), the estimate for the magnetic fileds during the Electroweak Phase Transition raises to $10^{32} - 10^{33}$ Gauss, according to [3]. If this is the case, the dynamical mass is of the order of 100 GeV and we believe that this possibility deserves further study in connection with Cosmology and the Electroweak Phase Transition.

Acknowledgements

This work has been within the TMR project "Finite temperature phase transitions in particle Physics", EU contract number: FMRX-CT97-0122. The authors would like to acknowledge financial support from the TMR project. Illuminating discussions with G.Triantafillou are gratefully acknowledged.

A Polarization tensor in magnetic field (d=2+1)

The free photon propagator in the presence of a magnetic field is [12]

$$D_{\mu\nu}(q) = \frac{1}{q^2}\left(g^{\parallel}_{\mu\nu} - \frac{q^{\perp}_{\mu}q^{\perp}_{\nu}}{q^2_{\perp}} - \frac{q_\mu q_\nu}{q^2}\right) + \frac{1}{q^2}\left(g^{\perp}_{\mu\nu} + \frac{q^{\perp}_{\mu}q^{\perp}_{\nu}}{q^2_{\perp}}\right) + \lambda\frac{q_\mu q_\nu}{q^4} \tag{59}$$

where λ is the gauge fixing parameter. Because of the projection operator $(1 - i\gamma^1\gamma^2 sg(eB))/2$ that we have in the fermion propagators (6) and (20), the components of $D_{\mu\nu}$ which include only the transverse coordinates $(1, 2)$ will not play any role in the Schwinger-Dyson equation. Therefore in the LLL approximation the free photon propagator will be

$$D^{LLL}_{\mu\nu}(q) = -\frac{i}{q^2}\left(g^{\parallel}_{\mu\nu} - \frac{q_\mu q_\nu}{q^2}\right) - i\lambda\frac{q_\mu q_\nu}{q^4} \tag{60}$$

We show now that the corrections to the photon propagator in dimension 2+1 need not be taken into account in the LLL approximation. In Euclidean space-time the one-loop level polarization tensor is given by [14, 21]

$$\Pi_{\mu\nu}(p) = (p^2\delta_{\mu\nu} - p_\mu p_\nu)N_0(p) + (p^2_{\perp}\delta^{\perp}_{\mu\nu} - p^{\perp}_{\mu}p^{\perp}_{\nu})N_1(p) \tag{61}$$

where

$$\begin{aligned} N_0(p) &= -\frac{\alpha}{2\sqrt{\pi}}\int_0^\infty \frac{ds}{s}\int_{-1}^{1} dv e^{-s\phi_0}\frac{z}{\sinh(z)}[\cosh(zv) - v\coth(z)\sinh(zv)] \\ N_1(p) &= -\frac{\alpha}{2\sqrt{\pi}}\int_0^\infty \frac{ds}{s}\int_{-1}^{1} dv e^{-s\phi_0}\frac{2z}{\sinh^3(z)}[\cosh(z) - \cosh(zv)] - N_0(p) \end{aligned} \tag{62}$$

with $z = |eB|s$ and

$$\phi_0 = m^2 + \frac{1 - v^2}{4}p_0^2 + \frac{\cosh(z) - \cosh(zv)}{2z\sinh(z)}p^2_{\perp} \tag{63}$$

We will need only the component $\Pi_{00}(p)$ in the LLL approximation, thus we only need to look at $N_0(p)$ in the strong field limit $|eB| >> s^{-1}$. Making an expansion for $z >> 1$ we obtain after the interation over v :

$$N_0(p) = -2\frac{\alpha}{\sqrt{\pi}}\int_0^\infty \frac{ds}{s} z e^{-s(m^2+p_0^2/4)-z}\left(1+\mathcal{O}(z^{-1})\right) \tag{64}$$

which finally leads to:

$$N_0(p) = -\frac{2\alpha}{\sqrt{\pi|eB|}}\int_0^\infty d\sigma\sqrt{\sigma}e^{-\sigma}\left[1+\mathcal{O}\left(\frac{p_0^2+m^2}{|eB|}\right)\right] \tag{65}$$

We see then that the one-loop polarization tensor vanishes as $\alpha|eB|^{-1/2}$.

References

[1] G.K.Savvidy, Phys.Lett. B71 (1977) 133.

[2] P.Salabura and al, Phys.Lett.B245 (1990), 153; D.G.Caldi, A.Chodos, Phys.Rev.D36 (1987), 2876; Y.J.Ng, Y.Kikuchi, Phys.Rev. D36 (1987) 2880.

[3] J.Ambjorn, P.Olesen, hep-ph/9304220, in the *Proceedings of the 4th Hellenic School on Elementary Particle Physics*, Corfu, September 1992.

[4] A.Salam, J.Strathdee, Nucl.Phys.B90 (1975) 203; A.D.Linde, Phys.Lett.B62 (1976), 435; B.J.Harrington, H.K.Shepard, Nucl.Phys.B105 (1976), 527.

[5] M.Giovannini, M.E.Schaposhnikov, Phys.Rev.D57 (1998), 2186; K.Kajantie, M.Laine, J.Peiser, K.Rummukainen, M.E.Shaposhnikov, Nuc.Phys. B544 (1999), 357; V.Skalozub, M.Bordag, hep-ph/9807510, hep-ph/9904333.

[6] T.Vachaspati, Phys.Lett. B265 (1991) 258; K.Enqvist, P.Olesen Phys.Lett.B319 (1993) 178; A.Ruzmaikin, A.Shukurov, D.Sokoloff, *Magnetic Fields of Galaxies*, Kluwer Dordrecht (1988), P.H.Brandenberger, A.-C.Davis, A.M.Matheson, M.Troden, Phys.Lett.B293 (1992), 287.

[7] R.Shankar, Phys.Rev.Lett.63 (1989), 203; N.Dorey, N.E.Mavromatos, Nuc.Phys.B386 (1992), 614.

[8] K.Farakos, N.E.Mavromatos, Int.Journ.Mod.Phys.B12 (1998), 809.

[9] V.P.Gusynin, V.A.Miransky, I.A.Shovkovy, Nucl.Phys.B563 (1999), 361.

[10] V.P.Gusynin, V.A.Miransky, L.A.Shovkovy, Nucl.Phys.B462 (1996), 249; C.N.Leung, Y.J.Ng, A.W.Ackley, Phys. Rev. D54 (1996) 4181.

[11] W.Dittrich, M.Reuter, *Effective Lagrangians in Quantum Electrodynamics*, Springer, 1985; G.Callucci, R.Ragazzon, J.Phys.A 27 (1994), 2161; V.P.Gusynin, V.A.Miransky, I.A.Shovkovy, Nuc.Phys.B462 (1996), 249.

[12] A.V.Shpagin, hep-th/9611412.

[13] T.Appelquist, D.Nash, L.C.R.Wijewardhana, Phys.Rev.Lett.60 (1988),2575;
R.D.Pisarsky, Phys.Rev. **D29** (1984), 2423.

[14] K.Farakos, G.Koutsoumbas, N.E.Mavromatos, A.Momen, Phys.Rev.D61 (2000), 45005.

[15] E.J.Ferrer, V. de la Incera, hep-th/9910035.

[16] J.Schwinger, Phys.Rev.82 (1951), 664.

[17] A.Chodos, K.Everding, D.Owen, Phys.Rev.D42, (1990), 2881.

[18] D.-S.Lee, C.N.Leung, Y.J.Ng, Phys.Rev.D55, (1997), 6504.

[19] V.A.Miransky, *Dynamical symmetry breaking in quantum field theories*, World Scientific, 1993.

[20] K.Farakos, G.Koutsoumbas, N.E.Mavromatos, Phys.Lett.B431 (1998) 147.

[21] W.Tsai, Phys.Rev.D10 (1974) 2699.

[22] K.Farakos, N.E.Mavromatos, Phys.Rev. B57 (1998) 3017.

[23] K.Krishana et al, Science 277 (1997) 83.